



Article

Synthesis, Structure, Spectral-Luminescent Properties, and Biological Activity of Chlorine-Substituted *N*-[2-(Phenyliminomethyl)phenyl]-4-methylbenzenesulfamide and Their Zinc(II) Complexes

Anatolii S. Burlov ¹, Valery G. Vlasenko ², Maxim S. Milutka ¹, Yurii V. Koshchlenko ¹, Nadezhda I. Makarova ¹, Vladimir A. Lazarenko ³, Alexander L. Trigub ³, Alexandra A. Kolodina ¹, Alexander A. Zubenko ⁴, Anatoly V. Metelitsa ¹, Dmitrii A. Garnovskii ⁵, Alexey N. Gusev ^{6,*} and Wolfgang Linert ⁷

- ¹ Institute of Physical and Organic Chemistry, Southern Federal University, 344090 Rostov-on-Don, Russia
² Institute of Physics, Southern Federal University, 344090 Rostov-on-Don, Russia
³ National Research Centre "Kurchatov Institute", 123182 Moscow, Russia
⁴ North-Caucasian Zonal Scientific Research Veterinary Institute, Branch of the Federal State Budget Scientific Institution "Federal Rostov Agricultural Research Centre", 346421 Novocherkassk, Russia
⁵ Southern Scientific Center of Russian Academy of Sciences, 344006 Rostov-on-Don, Russia
⁶ General Chemistry Department, Crimean Federal University V.I. Vernadsky, 295007 Simferopol, Russia
⁷ Institute of Applied Physics, Vienna University of Technology, Wiedner Hauptstraße 8-10, 1040 Vienna, Austria
* Correspondence: galex0330@gmail.com; Tel.: +7-978-723-4813



Citation: Burlov, A.S.; Vlasenko, V.G.; Milutka, M.S.; Koshchlenko, Y.V.; Makarova, N.I.; Lazarenko, V.A.; Trigub, A.L.; Kolodina, A.A.; Zubenko, A.A.; Metelitsa, A.V.; et al. Synthesis, Structure, Spectral-Luminescent Properties, and Biological Activity of Chlorine-Substituted *N*-[2-(Phenyliminomethyl)phenyl]-4-methylbenzenesulfamide and Their Zinc(II) Complexes. *Int. J. Mol. Sci.* **2022**, *23*, 15259. <https://doi.org/10.3390/ijms232315259>

Academic Editor: Zdeněk Trávnický

Received: 2 November 2022

Accepted: 30 November 2022

Published: 3 December 2022

Publisher's Note: MDPI stays neutral with regard to jurisdictional claims in published maps and institutional affiliations.



Copyright: © 2022 by the authors. Licensee MDPI, Basel, Switzerland. This article is an open access article distributed under the terms and conditions of the Creative Commons Attribution (CC BY) license (<https://creativecommons.org/licenses/by/4.0/>).

Abstract: New azomethine compounds of 2-(*N*-tosylamino) benzaldehyde or 5-chloro-2-(*N*-tosylamino) benzaldehyde and the corresponding chlorine-substituted anilines, zinc(II) complexes based on them have been synthesized. The structures of azomethines and their complexes were determined by elemental analysis, IR, ¹H NMR, X-ray spectroscopy, and X-ray diffraction. It is found that all ZnL₂ complexes have a tetrahedral structure according to XAFS and X-ray diffraction data. The photoluminescent properties of azomethines and zinc complexes in methylene chloride solution and in solid form have been studied. It is shown that the photoluminescence quantum yields of solid samples of the complexes are an order of magnitude higher compared to the solutions and range from 11.34% to 48.3%. The thermal properties of Zn(II) complexes were determined by thermal gravimetric analysis (TGA) and differential scanning calorimetry. The TGA curves of all the compounds suggest their high thermal stability up to temperatures higher than 290 °C. The electrochemical properties of all complexes were investigated by the cyclic voltammetry method. The multilayered devices ITO/PEDOT:PSS/NPD/Zn complex/ TPBI/LiF/Al with wide electroluminescence (EL) color range spanning the range from bluish-green (494 nm) to green (533 nm) and the high values of brightness, current and power efficiency were fabricated. The biological activity of azomethines and zinc complexes has been studied. In the case of complexes, the protistocidal activity of the zinc complex with azomethine of 5-chloro-2-(*N*-tosylamino)benzaldehyde with 4-chloroaniline was two times higher than the activity of the reference drug toltrazuril.

Keywords: azomethines; zinc(II) complexes; photoluminescence; electroluminescence; biological activity

1. Introduction

For a long time, the interest of researchers in the synthesis and study of the physicochemical properties of new Schiff bases by salicylaldehyde derivatives and transition metal complexes based on them has not faded [1–3]. Significant progress in this area is primarily due to the practical importance of these compounds. In particular, these compounds demonstrate a wide range of biological activity [4,5] exhibiting antifungal [6,7], antibacterial [6–8], anticancer [9–13], and antiviral [14] properties, which determines their demand by medicine, veterinary medicine, and agriculture.

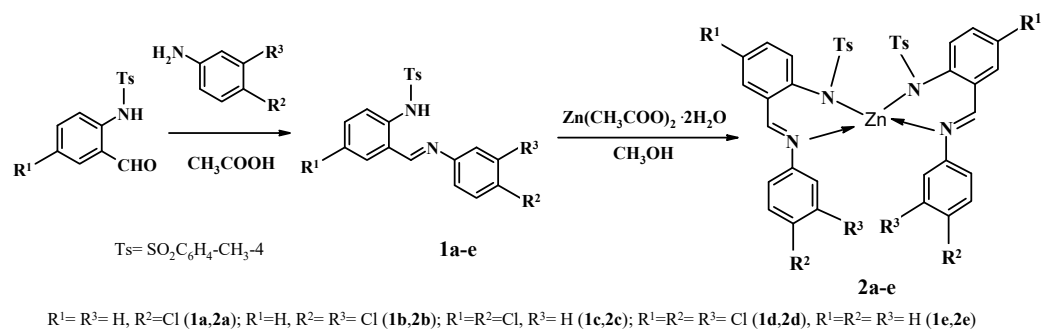
Particular attention is drawn to zinc complexes of chelating azomethine ligands, owing to their photo- and electroluminescent properties, which allow their use as emitting layers in OLED devices, which have many advantages in terms of power consumption, brightness, and color compared to traditional sources [15–21]. These complexes have a number of advantages, having high thermal stability, volatility, and solubility; they are relatively simple for synthesis, non-toxic and cheap. In addition, varying the nature of substituents in azomethine ligands makes it possible to fine-tune the luminescent characteristics of zinc complexes based on them. For example, based on Zn(II) complexes containing salicylaldiminate ligands, blue, greenish-white, and red emitters for organic photoelectronics with good stability and efficiency have been obtained [22,23]. Of particular interest are the Zn(II) complexes of azomethine ligands of 2-(*N*-tosylamino)benzaldehyde [24,25] and 3-methyl-1-phenyl-4-formylpyrazol-5-one [26–30] derivatives. Replacing the hydroxy group in the aldehyde fragment of azomethines with a 2-tosylamino group with the formation of the MN₄ coordination site leads to an increase in thermal stability (m.p. increases by about 50–100 °C) [7,24,31–33] and solvent resistance of complexes as compared to azomethine complexes based on salicylic aldehydes. In addition, the introduction of chlorine atoms into position 5 of the 2-(*N*-tosylamino)benzaldehyde fragment promotes an increase in the solubility of both azomethines and complexes based on them. Zinc complexes based on azomethine ligands of 2-(*N*-tosylamino)benzaldehyde fluoresce in the blue region of the spectrum $\lambda_{PL} = 428\text{--}433\text{ nm}$ and have a high fluorescence quantum yield $\varphi > 0.20$, which makes them promising objects as an active emission layer of OLED.

Previously [34–36], we obtained a series of zinc complexes of bidentate azomethine ligands of halogenated 2-hydroxybenzaldehydes derivatives, and studied their structure, spectral-luminescent properties, and biological activity. In continuation of [35,36], we synthesized a similar series of azomethine compounds of 2-(*N*-tosylamino)benzaldehyde or 5-chloro-2-(*N*-tosylamino)benzaldehyde and the corresponding chlorine-substituted anilines, and zinc(II) complexes based on them. The main goal of this work was to study the effect of the halogen substituent in the amine and aldehyde fragments in zinc complexes on their photoluminescent properties and biological activity.

2. Results and Discussion

2.1. Synthesis of Azomethines and Their Zinc Complexes

Azomethine compounds **1a–e** were obtained by condensation of 2-(*N*-tosylamino)benzaldehyde or 5-chloro-2-(*N*-tosylamino)benzaldehyde and the corresponding chloro-substituted anilines in glacial acetic acid (Scheme 1).



Scheme 1. Synthesis of azomethines **1a–e** and zinc complexes **2a–e**.

2.2. Elemental Analysis and Spectroscopic Data

The structure of azomethines **1a–e** was established by elemental analysis, IR, and ¹H NMR spectroscopy. All of them are finely crystalline substances of white color with m.p. from 133 °C to 182 °C. The IR spectra of compounds **1a–e** show absorption bands $\nu(\text{CH}=\text{N})$ in the region 1614–1620 cm⁻¹, $\nu(\text{asSO}_2)$ in the region 1317–1343 cm⁻¹ and $\nu(\text{sSO}_2)$ at 1155–1162 cm⁻¹.

The ^1H NMR spectra of azomethines **1a–e** contain signals of all protons corresponding to their structures. The signals of the protons of the NH groups of the aldehyde fragments appear as a singlet in the range of 11.62–12.57 ppm, and the signals of the protons of the CH=N groups in the range of 8.62–8.76 ppm.

The synthesis of zinc bis-chelates **2a–e** was carried out by refluxing the corresponding azomethine **1a–e** and a methanol solution of zinc acetate dihydrate in a 2:1 molar ratio in a mixture of methanol: chloroform (1:1) (Scheme 1). All complexes are yellow crystalline substances with high melting points from 273 °C to 311 °C. According to the elemental analysis data, zinc complexes **2a–e** have the composition ZnL_2 . In the IR spectra of zinc complexes **2a–e**, the absorption bands $\nu(\text{CH}=\text{N})$ are observed at 1605–1611 cm^{-1} , shifting to the low-frequency region by 3–13 cm^{-1} , compared to the **1a–e**, and the absorption bands $\nu(\text{asSO}_2)$ and $\nu(\text{sSO}_2)$ are shifted to the low-frequency region by 22–43 cm^{-1} to 1285–1302 cm^{-1} in the case of $\nu(\text{asSO}_2)$ and by 19–23 cm^{-1} to 1131–1143 cm^{-1} in the case of the band $\nu(\text{sSO}_2)$. In the ^1H NMR spectra of complexes **2a–e**, the proton signals of the NH groups of **1a–e** disappear. The proton signals of CH=N groups in **2a–e** are slightly shifted downfield by 0.02–0.15 ppm compared to **1a–e** and appear at 8.74–8.78 ppm. Such changes observed in the IR and ^1H NMR spectra of zinc complexes **2a–e** are characteristic of the formation of chelate structures [24,25,31,34].

2.3. X-ray Absorption Spectroscopy

The local atomic structure of the nearest atomic environment of zinc ions in complexes **2a–d** was established from X-ray absorption spectroscopy data from the XANES and EXAFS analysis of Zn K absorption edges. Figure 1 shows normalized XANES and the corresponding MFT EXAFS for all compounds. It can be noted that the positions and shapes of the Zn K absorption edges **2a–d** are very close to each other (Figure 1a), indicating a similar environment of zinc ions in these compounds. The XANES of complexes **2a–d** lack the pre-edge peak A due to the filled 3d shell of Zn(II). The intense peak C (white line) corresponds to the maximum of the X-ray absorption spectrum and has the same energy position for all K absorption edges of complexes **2a–d**.

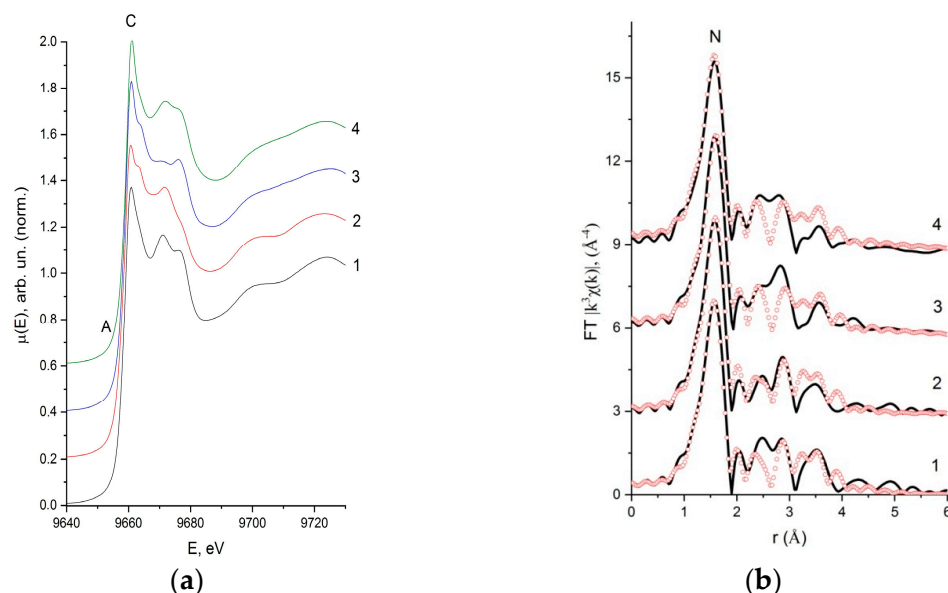


Figure 1. Normalized XANES spectra (a) and MFT EXAFS (b) of Zn K-edges for the complexes **2a** (1), **2b** (2), **2c** (3), **2d** (4), experiment—solid black line, best-fit theory—empty red circles.

Quantitative characteristics of the coordination polyhedron in **2a–d** were obtained from the EXAFS analysis of the Zn K-edges. Figure 1b shows the modules of Fourier transform (MFT) of EXAFS of these compounds. All MFTs have the main peak at $r = 1.51$ – 1.53 \AA , which corresponds to the scattering of a photoelectron wave by the nearest

coordination sphere (CS) of the nitrogen atoms of the ligands. The MFT peaks at large values of $r > 2.5 \text{ \AA}$ are associated with subsequent CSs containing various ligand atoms, mainly the carbon atoms, as well as oxygen and sulfur of the tosylamine fragments of the ligands. As a result of the performed EXAFS model calculations, it was found that the nearest environment of zinc ions in all complexes **2a–d** is very close and consists of four nitrogen atoms with average distances Zn ... N about 1.92 \AA , Zn ... N about 2.01 \AA (Table 1). The obtained values of the Debye-Waller factors of about 0.0030 \AA^2 are typical for such Zn ... N distances in coordination compounds with similar structures [36].

Table 1. Parameter ¹ of the local structure around the zinc ions in complexes **2a–d**, obtained from EXAFS analysis of Zn *K*-edges.

Compound	Bond	N	R, \AA	σ^2 , \AA^2	Q, %
2a	Zn–N	2	1.98	0.0030	1.3
	Zn–N	2	2.06	0.0030	
2b	Zn–N	2	1.98	0.0030	1.2
	Zn–N	2	2.06	0.0030	
2c	Zn–N	2	1.98	0.0030	1.3
	Zn–N	2	2.06	0.0030	
2d	Zn–N	2	1.99	0.0030	1.6
	Zn–N	2	2.05	0.0030	

¹ N—coordination numbers, R—interatomic distances, ² σ^2 —Debye-Waller factors, Q—is the integral fit quality factor. EXAFS fitting: $\Delta r = 1.00\text{--}1.98 \text{ \AA}$.

2.4. A Single-Crystal X-ray Diffraction

The structures of **2d** and **2a** complexes were established by X-ray diffraction. The structure of complexes **2a**, **2d**, and the structure of crystal **2a** along the [100] axis are shown in Figure 2. The complexes **2a** and **2d** with the metal-to-ligand ratio 1:2 are described by an idealized C_2 (2) symmetry and crystallize in the C_2/c space group with the chemical formulae $C_{40}H_{32}Cl_2N_4O_4S_2Zn$ and $C_{40}H_{28}Cl_6N_4O_4S_2Zn$, respectively. The Zn ions have an oxidation state of 2+ and biccapped tetrahedral coordination environment “4 + 2” by four N atoms from the tosylamino and imine groups [Zn1–N1 1.9763(14) \AA , Zn1–N2 2.0507(14) \AA for **2a** and Zn1–N1 1.98763(3) \AA , Zn1–N2 2.04076(3) \AA for **2d**], and additional weaker interactions with two O atoms from sulfo groups [Zn1...O1 2.66919(13) \AA for **2a** and Zn1...O1 2.67283(4) \AA for **2d**]. The average values of bond lengths coincide with the average values of such bonds from the CSD [37]. The crystal packings of analyzed complexes are enhanced by intermolecular hydrogen bonds O1...H6'–C6'/O1'...H6–C6 and O2...H9'–C9'/O2'...H9–C9 for **2d/2a**, respectively. The distances and angles for these hydrogen bonds for **2d/2a** are [C...O 3.17985(4)/3.199(2) \AA , H...O 2.40149(4)/2.3041(13) \AA , $\angle C-H...O$ 138.9652(8)/161.19(11) $^\circ$] for the first pair of hydrogen bonds, and [C...O 2.99820(6)/3.078(2) \AA , H...O 2.35724(4)/2.4076(15) \AA , $\angle C-H...O$ 124.3966(10)/128.91(11) $^\circ$] for the second pair. The crystal structure of **2a** (Figure 3) is strengthened by π – π interactions between benzene rings of the tosyl fragments of ligands with a 3.927 \AA centroid-centroid distance and 1.904 \AA shift distance.

2.5. The Electron Absorption and Photoluminescence Spectra

The absorption and photoluminescence (PL) spectra of zinc complexes **2a–e** in methylene chloride solution (Figure 4) and in solid form (Figure 5) were studied. In the UV-Vis spectra of complexes **2a–e** in a solution of CH_2Cl_2 , two absorption bands are observed in the region $\lambda_{max} = 306\text{--}312 \text{ nm}$ and $\lambda_{max} = 385\text{--}400 \text{ nm}$ (Table 2). When excited into long-wavelength absorption bands, fluorescence is observed with band maxima in the region $\lambda_{PL} = 488\text{--}509 \text{ nm}$ (Figure 4). The Stokes shift is between 103 and 197 nm. The quantum yields ϕ of PL in CH_2Cl_2 solutions are insignificant and range from $\phi = 0.029$ to $\phi = 0.062$. As can be seen from Table 2, the introduction of a second chlorine atom into the aniline fragment of the ligand leads to a slight increase in the quantum yield of PL. The maxima

of the PL bands of solid samples of complexes are shifted to the long-wavelength region of the spectrum compared to solutions. The PL quantum yields of solid samples of the complexes are an order of magnitude higher than those of solutions and range from 11.34% to 48.3%. The introduction of a chlorine atom into position 5 of the aldehyde fragment leads to the bathochromic shift of the fluorescence band of solid samples of the complexes and a decrease in the fluorescence quantum yield (Table 2).

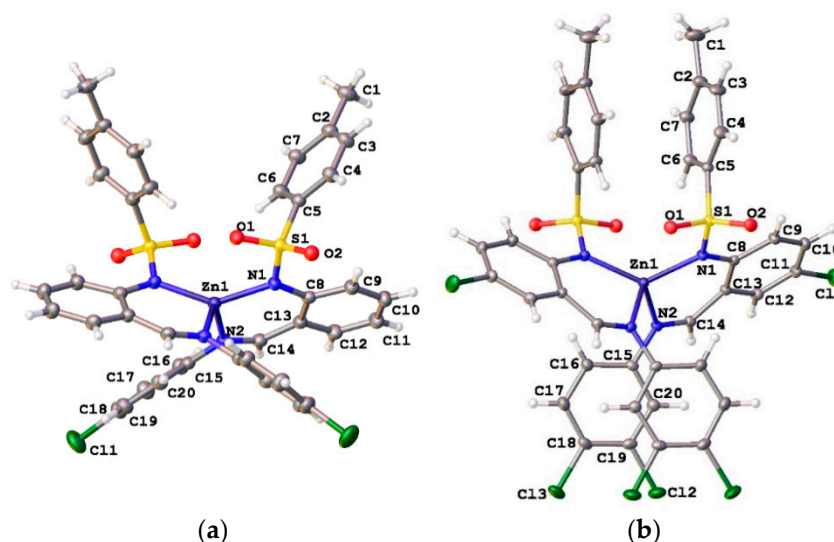


Figure 2. Molecular structures of complexes **2a** (a) and **2d** (b). Displacement ellipsoids are shown at the 50% probability level.

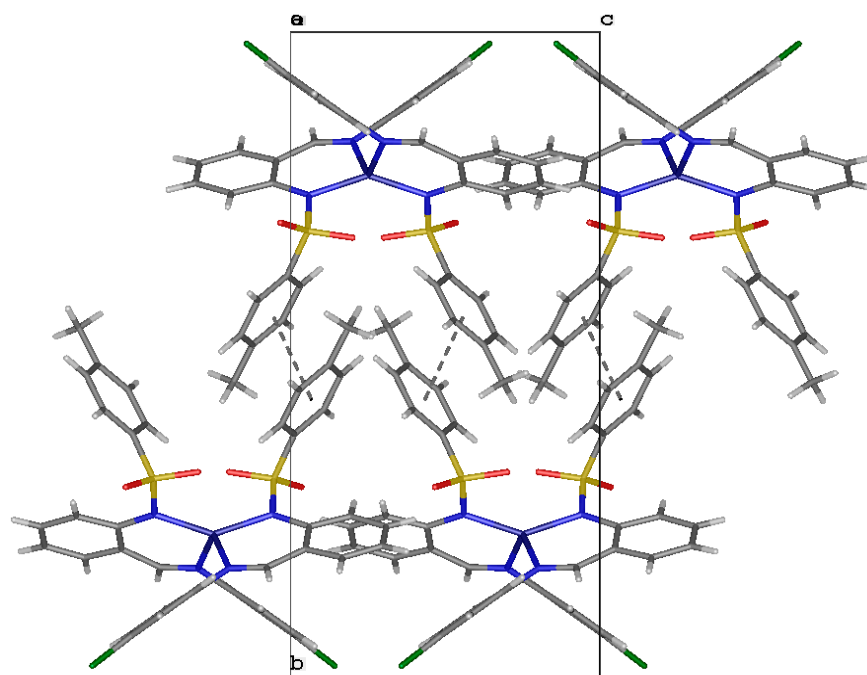


Figure 3. Arrangement of neighboring molecules in the crystal structure of **2a** showing the aromatic π - π interactions; a view along the [100] direction.

It should be noted that compared with zinc complexes based on 5-chloro-2-hydroxybenzaldehyde [35], the replacement of the hydroxy group of the aldehyde fragment with the tosylamino group (**2c**) leads to a hypsochromic shift of the PL bands by 4 nm (in CH_2Cl_2 solution) and 23 nm (solid-state) and an increase in PL quantum yields from 2% to 5% (in CH_2Cl_2 solution) and from 14.7% to 21.4% (solid-state).

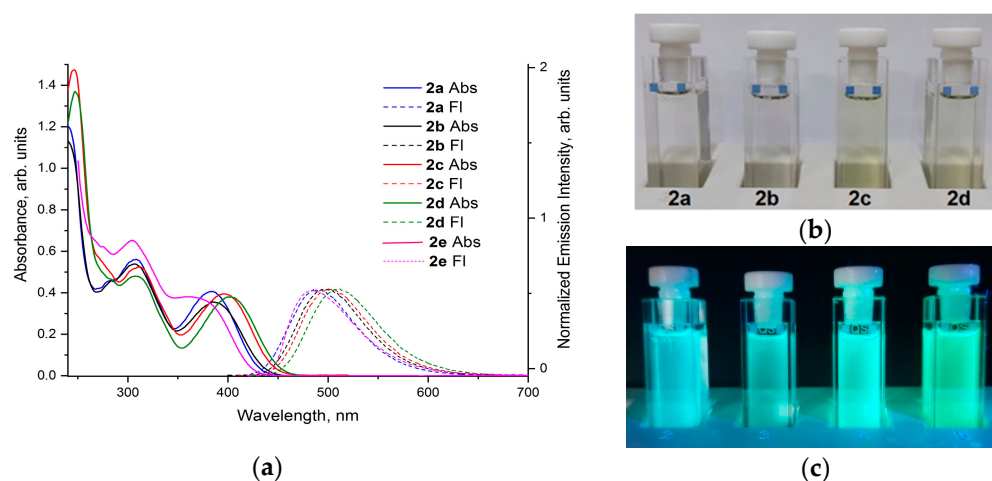


Figure 4. The UV-Vis spectra (solid lines) and normalized emission ($\lambda_{\text{ex}} = 390\text{--}400$ nm) spectra (dash lines) of **2a–e** in CH_2Cl_2 solution (a). The photographs of **2a–d** in CH_2Cl_2 solutions: before radiation (no emission) (b); during radiation (photoluminescence, $\lambda_{\text{ex}} = 365$ nm) at r.t. (c).

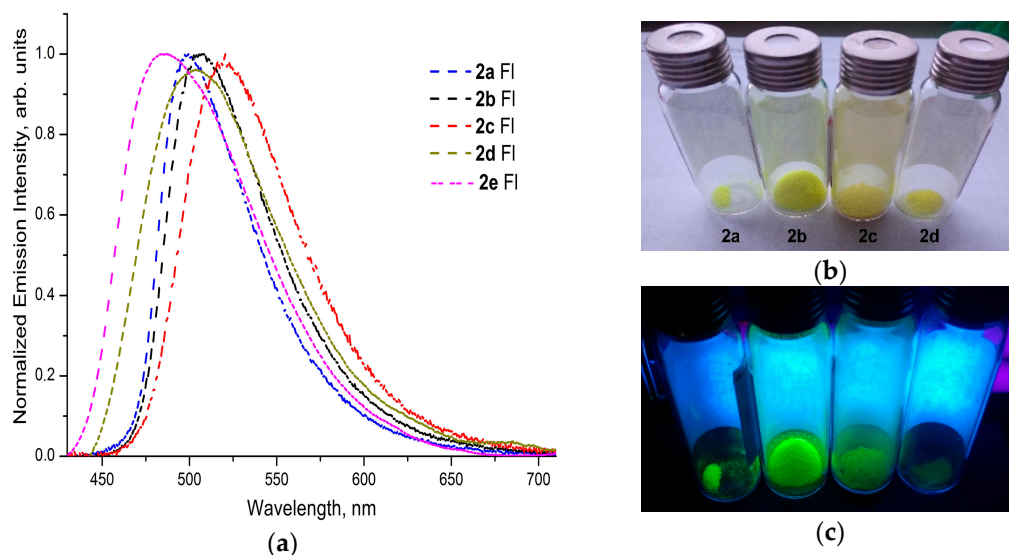


Figure 5. The normalized emission ($\lambda_{\text{ex}} = 390\text{--}400$ nm) spectra of **2a–e** in solid state (a). The photographs of **2a–d** in the solid state: before radiation (no emission) (b); during radiation (photoluminescence, $\lambda_{\text{ex}} = 365$ nm) at r.t. (c).

2.6. Thermal and Electrochemical Properties

The thermal stability of luminescent complex is very important for OLED applications, which are directly related to device performance such as efficiency, lifetime, etc. The thermal properties of title complexes **2a–e** were determined by thermal gravimetric analysis (TGA) and differential scanning calorimetry (DSC) under a nitrogen atmosphere. The main parameters of thermal transitions are shown in Table 3. The TGA curves of all compounds suggest high thermal stability estimated by the start of the decomposition of complexes (T_d , corresponding to 2% weight loss) (Figure S1). No loss of adsorbed or coordinated solvate molecules was observed for all complexes, which is consistent with EA data. The complexes only had a 2% weight loss at 340 (**2a**), 305 (**2b**), 335 (**2c**), and 290 (**2d**) °C. Complexes **2b** and **2d** having substitutions in the *meta*-position of aldehyde moiety, exhibited lower T_d . Upon further heating, decomposition starts above 390–420 °C with a series of complicated weight losses, which continue until heating ends at 670–700 °C. Detailed decomposition mechanisms of the four complexes are too complex to be explained. The remaining weight agrees with the theoretical value calculated by taking zinc oxide as the final product.

Table 2. UV-Vis and PL data of **2a–e** in CH₂Cl₂ and solid state at 293 K.

No.	Structure	Absorption λ_{\max} , nm (ϵ , 104 M ⁻¹ cm ⁻¹)	Photoluminescence, Solution/Solid State		
			Excitation λ_{\max} , nm	Emission λ_{\max} , nm	φ *
2a		308 (2.81), 385 (2.04)	310, 385	488/499	0.032/0.391
2b		306 (2.70), 385 (1.78)	307, 386	497/507	0.054/0.483
2c		312 (2.62), 397 (2.00)	313, 397	500/520	0.050/0.214
2d		307 (2.40), 400 (1.90)	312, 398	511, 586/503	0.062/0.047
2e		306 (2.60), 370 (1.58)	310, 385	485/487	0.015/0.113

* PL quantum yield was determined using an integrating sphere of the C11347-01 Hamamatsu spectrometer. Excitation at 390 nm.

Table 3. Electrochemical and thermal properties of **2a–d** complexes.

Compound	T _m , °C	T _d , °C	T _g , °C	E(Ox), V	E(Red), V	E(HOMO), eV	E(LUMO), eV
2a	317	340	101	1.02	−0.58	−5.42	−2.59
2b	304	305	-	1.08	−0.72	−5.48	−2.72
2c	311	335	-	1.04	−0.62	−5.44	−2.68
2d	275	290	-	1.11	−0.68	−5.51	−2.79

The first DSC heating scans confirmed that complexes were obtained as crystalline materials with melting point (T_m) values of 317, 304, 311, and 275 °C for **2a–d**, respectively. The melting of the title complexes exhibits sharp endothermic peaks. No transition peaks associated with crystallization peaks were observed during the DSC cooling scans, which indicated the formation of glasses. In the second DSC heating scan, only complex **2a** exhibited glass transitions with glass transition temperatures (T_g) 101 °C. There was no evident glass-transition temperature (T_g) observed from 50 °C to 150 °C for the other compounds, which can be attributed to the more rigid structure due to strong intermolecular interactions.

The excellent thermal properties of **2a–d** inspired us to fabricate efficient OLEDs by vacuum thermal evaporation technique.

Further, we used cyclic voltammetry to investigate the electrochemical properties and determine the energy levels of title complexes. The electrochemical behavior was studied in dry acetonitrile (0.01 M solutions) by cyclic voltammetry (CV) measurement in a three-electrode cell system. The detailed electrochemical properties of the Zn(II) complexes are listed in Table 3. During the anodic scan, a monoelectronic and irreversible anodic wave with a peak maximum at 1.04–1.11 V corresponding to the oxidation of the Schiff base moieties is observed in the CV profiles. From the electrochemical and spectral data, the energies of the LUMO and HOMO levels of **2a–d** were estimated as listed in Table 3. According to the oxidation onset-potential values, the highest unoccupied molecular orbital (HOMO) energy levels E_{HOMO} were estimated to be -5.21 – -5.33 eV. The relative lower E_{HOMO} of **2a** and **2c** originated from the stronger electron-withdrawing ability of chlorine-atom in *meta*-position. Estimation of the LUMO energy values was carried out by the addition of an energy gap calculated from spectral data. LUMO levels are located in the range of -2.59 to -2.79 eV.

2.7. Electroluminescence Studies

In order to evaluate the electroluminescent (EL) properties of the **2a–d** complexes, the following multilayered devices ITO/PEDOT:PSS/NPD/**2a–d**/TPBI/LiF/Al. were fabricated in which **2a–d** act as the emitters named: device A—**2a**; device B—**2b**; device C—**2c**; device D—**2d**, respectively. PEDOT:PSS (poly(3,4-ethylenedioxythiophene) polystyrene sulfonate)—hole injector. NPD (N,N'-Di(1-naphthyl)-N,N'-diphenyl-(1,1'-biphenyl)-4,4'-diamine)—hole transporter. TPBI 1,3,5-tris(N-phenylbenzimidazole-2-yl)benzene—electron transporter. LiF is used both to lower the energy barrier between the LUMO level of the Zn complex and the electron emission work from aluminum and to prevent Al aluminum atoms from entering the emitting layer when forming the cathode. Aluminum served as the cathode

All devices exhibited the typical diode characteristics. The light turn-on voltage for all devices was in the range of 4.5–7 V. All devices emitted a greenish-blue or green light (Figure 6a). Figure 6b shows the normalized EL spectra of title devices. In accordance with their PL spectra, a wide EL color range spanning from bluish-green (494 nm for **2a**) to green (533 nm for **2d**) was obtained for these devices. The EL spectra of these devices are almost invariant of the applied voltages, and it is clear that the EL spectra of the **2a–b** complex matched well with their PL in terms of spectral profile and position, confirming that no emission signal from electroplex or excimer/exciple has appeared in these devices under electroexcitation. From the EL spectra, it was concluded that the peak position of the emitted light is independent of the applied voltage. Complexes **2a** and **2c**, which contain only one Cl-atom in the aldehyde fragment of the ligand, show better performance than complexes **2b** and **2d** which have two Cl substituents. For example, the luminescence intensity of device A-D increases with increasing voltage reaching a brightness of more than 1545 Cd/m^2 at 18 V in the case of device A and 1007 Cd/m^2 at 17 V in the case of device C, while the brightness of the other devices was below 1000 Cd/m^2 at 18 V. Further increasing of bias voltage leads to fast destruction of cells. Figure 6c,d show the current-voltage and brightness-voltage characteristics of the created OLED structures, and Table 4 presents the electroluminescence parameters. Device A also shows the highest in this series maximum current and power efficiency of 2.7 cd/A, 1.7 lm/W. Maximum EQE was found to be 2.11 (A), 1.20 (B); 1.25 (C); 0.9 (D) %, respectively.

Although the luminance and efficiency values of the resulting devices do not reach the maximum values for close structures [29–31], these preliminary results suggest that the title complexes have the potential for use as emissive layers in organic light-emitting diodes. However, the device architecture needs to be improved, by using perhaps a different host matrix, with better electron-transporting properties.

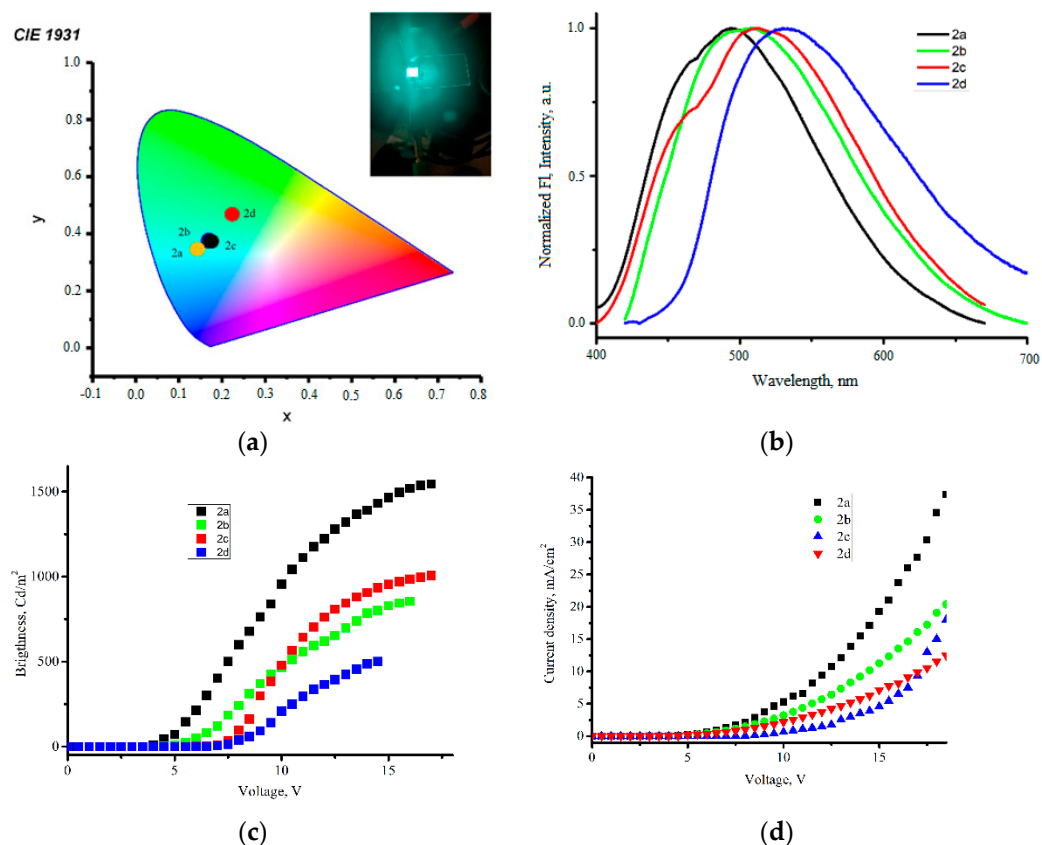


Figure 6. (a) Chromaticity coordinates of ELD on the base of complexes (inset: photo of device A); (b) Normalized EL spectra of OLEDs based on **2a–d**; (c) Luminance vs. voltage plot (d) Current density vs. voltage plot.

Table 4. Device performances of devices A–D.

Device	EL λ_{\max} , nm	CIE	Max. Brightness (Cd/m ²)	Current Efficiency Cd/A	Power Efficiency m/W	EQE, %
A	493	0.15:0.36	1542	2.7	1.7	2.11
B	509	0.19:0.42	854	1.9	1.5	1.20
C	511	0.20:0.44	1007	2.4	1.6	1.25
D	533	0.24:0.50	501	1.7	1.4	0.90

2.8. The Biological Activity

The biological activity of azomethine compounds **1a–e** and zinc(II) complexes **2a–e** based on them was studied. It was found that all azomethines **1a–e** and the zinc complexes **2a–e** show no fungistatic activity against *Penicillium italicum* (Table 5). Azomethines **1b**, **1d**, and **1e** show antibacterial activity against *Staphylococcus aureus*, but their activity is 2.2 times weaker than that of the reference drug furazolidone in the case of azomethines **1b,d** containing two chlorine atoms in the amine moiety, and 1.3 times weaker in the case of azomethine **1e** containing no chlorine atoms.

Only azomethines **1a** and **1e** are active against *Escherichia coli*. The activity of azomethine **1a**, containing a chlorine atom in the amine part, is 2.3 times, and the activity of **1e** is 1.2 times weaker than that of furazolidone. In the case of complexes, the complexes **2a**, **2c**, **2d**, and **2e** show bacteriostatic activity against *Staphylococcus aureus*, but the activity of complexes **2a**, **2c**, **2d**, containing from one to three chlorine atoms in the ligand, is 2.2–2.5 times and the activity of complex **2e**, which does not contain chlorine atoms in the ligand, is 1.3 times weaker than that of furazolidone. With respect to *Escherichia coli*,

complexes **2c** and **2d** show activity 1.5–1.8 times, and complex **2e** is 1.3 times weaker than that furazolidone.

Table 5. Protistocidal, fungistatic and antibacterial activities of azomethines **1a–e** and zinc complexes **2a–e**.

Compound	Protistocidal Activity	Fungistatic Activity	Antibacterial Activity	
	<i>Colpoda steinii</i> , µg/mL	<i>Penicillium italicum</i> , Inhibition Zone Diameter, mm	<i>Staphylococcus aureus</i> 6538 P, Inhibition Zone Diameter, mm	<i>Escherichia coli</i> F50, Inhibition Zone Diameter, mm
1a	500	0	0	8
1b	250	0	9	0
1c	500	0	0	0
1d	250	0	9	0
1e	15.6	0	15	15
2a	>500	0	8	0
2b	>500	0	0	0
2c	31.25	0	9	12
2d	>500	0	8	10
2e	500	0	15	14
Baycox (Toltrazuril)	62.5	-	-	-
Fundazol	-	40	-	-
Furazolidone	-	-	20	18

It was found that compound **1e**, containing no chlorine atoms, has high protistocidal activity among azomethines (Table 5). Its activity is 4 times higher than the activity of the reference drug toltrazuril, whereas azomethines **1a–d** containing chlorine atoms at different positions of azomethine, show weak protistocidal activity, which is 4–8 times weaker than the activity of the reference drug toltrazuril. Among the complexes **2a–e**, the most active against *Colpodasteinii* is the complex **2c**, containing one chlorine atom in each of the aldehyde and amine parts of the ligand, whose activity is 2 times stronger than that of toltrazuril. The activity of complex **2e** is 8 times weaker than that of toltrazuril. Complexes **2a,b,d** did not show protistocidal activity.

When comparing the antibacterial activity of azomethines **1a–e** and their complexes **2a–e**, it was shown that complexes **2a,c**, containing one or two chlorine atoms in the ligand, showed activity against *Staphylococcus aureus* 2.2–2.5 times weaker than the reference drug, in contrast to the corresponding azomethines, which did not have such activity at all. Complex **2d**, containing two chlorine atoms in the amine part of the ligand, showed no activity compared to azomethine **1d**, which has antibacterial activity against *Staphylococcus aureus*. The activities of complexes **2d,e**, and the corresponding azomethines **1d,e** was found to be the same. With respect to *Escherichia coli*, complexes **2c,d** containing two or three chlorine atoms in the ligand showed activity 1.5–1.8 times weaker than the reference drug, in contrast to the corresponding azomethines, which did not possess such activity at all. Complex **2a** showed no activity compared to azomethine **1a**, which has antibacterial activity against *Escherichia coli*. The activities of complex **2e** and the corresponding azomethine **1e** were found to be the same. Complex **2b** and azomethine **1b** did not have the corresponding activity.

When comparing the protistocidal activity of azomethines **1a–e** with their complexes **2a–e**, it was found that the protistocidal activity of the complexes decreases compared to azomethines, with the exception of complex **2c**, which contains one chlorine atom in each of the aldehyde and amine parts of the ligand. Complex **2c** showed activity 16 times greater than the activity of the corresponding azomethine **1c** and 2 times greater than the activity of the reference drug toltrazuril.

It should be noted that complexes **2a,b**, having one or two chlorine atoms in the amine part of the ligand, did not show protistocidal activity, whereas antibacterial activity among these complexes was observed only in monochlorine-substituted **2a** against *Staphylococcus aureus*, which was 2.5 times weaker than that of the reference drug. The introduction of a chlorine atom into the aldehyde part of the ligand of the complex with the retention of halogens in the amine part led to an increase in the biological activity of complexes **2c,d**, in

particular, the zinc complex **2c** containing one chlorine atom in the aldehyde part and one chlorine atom in the amine part of the ligand, showed protistocidal activity 2 times higher than that of toltrazuril.

The replacement of a 2-hydroxybenzaldehyde fragment containing one or two chlorine atoms in azomethines with 2-(*N*-tosylamino)benzaldehyde or its 5-chloro derivative has no particular effect on the change in biological activity. This conclusion is consistent with previously published data for related azomethine compounds [38,39], where it was shown that the substitution of chlorine atoms in the aldehyde fragment of the 2-hydroxybenzaldimine ligand of zinc complexes has a poor effect on their antimicrobial properties against Gram-positive (*Staphylococcus aureus*), and Gram-negative (*Escherichia coli*) organisms compared to the unsubstituted ligand, and less antimicrobial activity of known antibiotics (eg Gentamycin or Amoxicillin). The protistocidal activity of the zinc complex with azomethine of 5-chloro-2-(*N*-tosylamino)benzaldehyde with 4-chloroaniline was 2 times higher than the activity of toltrazuril, while the complex of zinc azomethine of 2-hydroxybenzaldehyde with 4-chloroaniline did not exhibit this activity [35].

3. Materials and Methods

3.1. General Methods

Commercially available reagents were used as purchased without additional pretreatment and/or purification. The C, H, and N elemental analysis were carried out on a «EuroEA-3000» (EuroVektor) analyzer. The amount of the metal was determined by the gravimetric method. The melting temperature of the synthesized compounds was determined by the capillary method, and for complexes, **2a–2d** it was refined by DSC data. The IR spectra of the samples were recorded on a Varian 3100-FTIR Excalibur instrument in the range 4000–400 cm⁻¹ by the method of disturbed total internal reflection. The ¹H NMR spectra were recorded on a Varian Unity-300 instrument (300 MHz) in DMSO-*d*₆. The chemical shifts of the ¹H nuclei are given relative to the residual signals of the deuterated solvent. UV-Vis spectra were recorded for a 2.0 × 10⁻⁵ M solution with Agilent 8453 spectrophotometer. Photoluminescent spectra were recorded for a 5.0 × 10⁻⁶ M solution on a Varian Cary Eclipse fluorescence spectrophotometer. All spectra were recorded in dichloromethane (for spectroscopy, Acros Organics) solutions at room temperature. Fluorescence quantum yield determined relative to 3-methoxybenzanthrone in toluene as standard (φ = 0.1, excitation at 365 nm) [40]. Photoluminescent spectra in the solid state were recorded with Hamamatsu C11347-01 absolute PL quantum yield spectrometer. Absolute PL quantum yield was determined using an integrating sphere of the Hamamatsu C11347-01 spectrometer (excitation at 390 nm). TG and DSC experiments were performed on a STA6000 (PerkinElmer, Inc., Shelton, CT, USA) under a static nitrogen atmosphere. Cyclic voltammetry measurements for complexes **2a–d** were performed following the protocol described in ref [41].

The OLED devices were fabricated on glass substrates with 100 nm thickness ITO. Organic layers were sequentially deposited at a rate in the range of 0.1–0.3 nm/s onto the substrates by high-vacuum (10⁻⁵ mbar) thermal evaporation techniques. The shadow mask with 5 mm × 5 mm openings was used to define the cathodes. The evaporating speeds and thickness were monitored by quartz oscillators. All of the measurements were carried out in an ambient atmosphere at room temperature after a vacuum break. The current density–luminance–voltage characteristics of the OLEDs were measured by the Keithley source measurement unit with a calibrated silicon photodiode. Electroluminescence spectra were taken by a multichannel S2000 Ocean Optics spectrometer. All measurements were carried out in an ambient atmosphere at room temperature.

The X-ray Zn K absorption edges of zinc complexes were obtained in the transmission mode at the Structural Materials Science station at the Kurchatov Synchrotron Center (Moscow) [42]. The energy of the electron beam, which was used as a source of X-ray synchrotron radiation, was 2.5 GeV at an average current of 100–120 mA. The X-ray absorption spectra were processed by standard procedures for extracting the background,

normalizing to the value of the K-edge jump, and extracting the atomic absorption μ_0 , after which the Fourier transform of the selected EXAFS (χ) spectrum was performed in the range of photoelectron wave vectors k from 2.5 to 12–13 \AA^{-1} with the weight function k^3 . The exact values of the nearest environment parameters of the zinc ion in the studied compounds were determined by nonlinear fitting of the parameters of the corresponding coordination spheres when comparing the calculated EXAFS with that extracted by the Fourier filtering method from the full absorption spectrum. This procedure was carried out using the IFFEFIT software package [43]. The phases and amplitudes of photoelectron wave scattering required for constructing the model spectrum were calculated using the FEFF7 program [44]. As the initial atomic coordinates necessary for calculating the scattering phases and amplitudes and further fitting, we used X-ray diffraction data for single crystals of metal complexes with a similar molecular structure from the Cambridge database. The fit quality function Q , which was minimized when finding the structure parameters of the nearest environment, was calculated using the formula:

$$Q^2 = \frac{\sum_{i=1}^m w(k_i) [k_i \chi_{\text{exp}}(k_i) - k_i \chi_{\text{th}}(k_i)]^2}{\sum_{i=1}^m w(k_i) [k_i \chi_{\text{exp}}(k_i)]^2}$$

where $w(k_i)$ is a weighting function, m is the number of experimental points, $\chi_{\text{data}}(R_i)$ and $\chi_{\text{th}}(R_i)$ are the EXAFS functions in the R -space.

The X-ray diffraction study of the crystals **2a** and **2d** was carried out at the “Belok/XSA” beamline of the Kurchatov Synchrotron Radiation Source [45,46]. Diffraction patterns were collected in direct geometry ($\theta = 0^\circ$) for **2a** and in a combination of direct and turned geometry ($\theta = 0^\circ$ for the first data set and $\theta = 26^\circ$ for the second data set) using a 1-axis MarDTB goniometer (φ -scanning mode with oscillation angle 1°) equipped with Rayonix SX165 CCD 2D positional sensitive CCD detector ($\lambda = 0.745 \text{ \AA}$). For the crystal of complex **2a**, data were obtained from two data sets, collected with different matrices of the orientation of the crystals, and for the crystal of complex **2d**, as described above. For each data set, ~180 diffraction frames were collected. All data were collected at 100 K.

The data were indexed and integrated by the XDS and XSCALE software suites [47]. The structures were solved by direct methods (intrinsic phasing) with SHELXT [48]. The structure model was investigated by Olex2 software [49] and refined by SHELXL [50] by a full-matrix least-squares method on F^2 with anisotropic displacements. As a result of combining two sets of data obtained in different geometries for the crystal of the complex **2d**, the obtained data are characterized by a larger maximum angle of 2θ and, as a result, better resolution and greater accuracy of the structural model, which leads to lower anisotropic displacement parameters. The crystallographic parameters and the refinement statistics for **2a** and **2d** are given in Tables S1–S9 (Supplementary Materials). Crystallographic data for **2a** and **2d** have been deposited with the Cambridge Crystallographic Data Center, CCDC 2203056 (**2a**), and CCDC 2203057 (**2d**). The supplementary crystallographic data can be obtained free of charge from the Cambridge Crystallographic Data Centre via www.ccdc.cam.ac.uk/data_request/cif (accessed on 7 October 2022.).

3.2. General Procedure for the Synthesis of Azomethines **1a–e**

A hot solution of 10 mmol of chlorine-substituted aniline in 5 mL of glacial acetic acid was added to a hot solution of 10 mmol of 2-(*N*-tosylamino)benzaldehyde or 5-chloro-2-(*N*-tosylamino)benzaldehyde in 10 mL of glacial acetic acid, the reaction mixture was stirred for 1 h at 100°C , then cooled to r. t. and 15 mL of ethanol were added. The precipitate that formed was filtered off, washed with ethanol, and dried in a vacuum oven at 100°C .

N-[2-[*I*-(4-Chlorophenyl)iminomethyl]phenyl]-4-methyl-benzenesulfonamide (**1a**) was obtained from 2.75 g (10 mmol) of 2-(*N*-tosylamino)benzaldehyde and 1.28 g (10 mmol) of 4-chloroaniline. Yield 3.62 g (94%), white powder, m.p. $133\text{--}134^\circ\text{C}$. IR spectrum, ν , cm^{-1} : 1618 (CH=N), 1342 (asSO₂), 1157 (sSO₂). ¹H NMR (DMSO-*d*₆), δ , ppm: 2.29 s(3H, CH₃),

7.18–7.23 m (1H, CH_{arom}), 7.30–7.37 m (4H, CH_{arom}), 7.41–7.46 m (2H, CH_{arom}), 7.54 dd (2H, CH_{arom}, 3J = 6.9 Hz, 4J = 2.1 Hz), 7.67 d (2H, CH_{arom}, 3J = 8.4 Hz), 7.76 d (1H, CH_{arom}, 3J = 7.2 Hz), 8.74 s (1H, CH=N), 12.29 s (1H, NH). Anal. calc. for C₂₀H₁₇ClN₂O₂S, %: C 62.41; H 4.45; N 7.28. Found, %: C 62.44; H 4.48; N 7.31.

N-[2-[(*E*)-(3,4-Dichlorophenyl)iminomethyl]phenyl]-4-methyl-benzenesulfonamide (**1b**) was obtained from 2.75 g (10 mmol) of 2-(*N*-tosylamino)benzaldehyde and 1.62 g of (10 mmol) 3,4-dichloroaniline. Yield 3.90 g (93%), White powder, m.p. 139–140 °C. IR spectrum, ν , cm⁻¹: 1616 (CH=N), 1343 (asSO₂), 1160 (sSO₂). ¹H NMR (DMSO-*d*₆), δ , ppm: 2.29 s (3H, CH₃), 7.23–7.32 m (4H, CH_{arom}), 7.39 d (1H, CH_{arom}, 3J = 7.5 Hz), 7.45–7.48 m (1H, CH_{arom}), 7.58 d (1H, CH_{arom}, 4J = 2.4 Hz), 7.66 d (2H, CH_{arom}, 3J = 8.4 Hz), 7.73 d (1H, CH_{arom}, 3J = 8.7 Hz), 7.78 dd (1H, CH_{arom}, 3J = 7.8 Hz, 4J = 1.2 Hz), 8.71 s (1H, CH=N), 11.92 s (1H, NH). Anal. calc. for C₂₀H₁₆Cl₂N₂O₂S, %: C 57.29; H 3.85; N 6.68. Found, %: C 57.25; H 3.81; N 6.64.

N-[4-Chloro-2-[(*E*)-(4-chlorophenyl)iminomethyl]phenyl]-4-methyl-benzenesulfonamide (**1c**) was obtained from 3.10 g (10 mmol) of 5-chloro-2-(*N*-tosylamino)benzaldehyde and 1.28 g (10 mmol) of 4-chloroaniline. Yield 3.77 g (90%), white powder, m.p. 181–182 °C. IR spectrum, ν , cm⁻¹: 1617 (CH=N), 1337 (asSO₂), 1162 (sSO₂). ¹H NMR (DMSO-*d*₆), δ , ppm: 2.29 s (3H, CH₃), 7.30–7.33 m (4H, CH_{arom}), 7.39 d (1H, CH_{arom}, 3J = 9.0 Hz), 7.52–7.56 m (3H, CH_{arom}), 7.64 d (2H, CH_{arom}, 3J = 8.1 Hz), 7.86 d (1H, CH_{arom}, 4J = 2.4 Hz), 8.66 s (1H, CH=N), 11.96 s (1H, NH). Anal. calc. for C₂₀H₁₆Cl₂N₂O₂S, %: C 57.29; H 3.85; N 6.68. Found, %: C 57.25; H 3.89; N 6.62.

N-[4-Chloro-2-[(*E*)-(3,4-dichlorophenyl)iminomethyl]phenyl]-4-methyl-benzenesulfonamide (**1d**) was obtained from 3.10 g (10 mmol) of 5-chloro-2-(*N*-tosylamino)benzaldehyde and 1.62 g (10 mmol) of 3,4-dichloroaniline. Yield 4.18 g (92%), white powder, m.p. 154–155 °C. IR spectrum, ν , cm⁻¹: 1614 (CH=N), 1317 (asSO₂), 1158 (sSO₂). ¹H NMR (DMSO-*d*₆), δ , ppm: 2.28 s (3H, CH₃), 7.25–7.32 m (3H, CH_{arom}), 7.37 d (1H, CH_{arom}, 3J = 9.0 Hz), 7.54 dd (2H, CH_{arom}, 3J = 8.1 Hz, 4J = 2.4 Hz), 7.63 d (2H, CH_{arom}, 3J = 8.4 Hz), 7.72 d (1H, CH_{arom}, 3J = 8.4 Hz), 7.85 d (1H, CH_{arom}, 4J = 2.7 Hz), 8.62 s (1H, CH=N), 11.62 s (1H, NH). Anal. calc. for C₂₀H₁₅Cl₃N₂O₂S, %: C 52.94; H 3.33; N 6.17. Found, %: C 52.90; H 3.37; N 6.21.

4-Methyl-*N*-[2-[(*E*)-phenyliminomethyl]phenyl]benzenesulfonamide (**1e**) was prepared from 2.75 g (10 mmol) of 2-(*N*-tosylamino)benzaldehyde and 0.93 g (10 mmol) of aniline in 30 mL of ethanol. Yield 3.33 g (95%), Light yellow needles, m.p. 99–100 °C. IR spectrum, ν , cm⁻¹: 2959 (NH), 1620 (CH=N), 1339 (asSO₂), 1155 (sSO₂). ¹H NMR (DMSO-*d*₆), δ , ppm: 2.29 s (3H, CH₃), 7.17–7.23 m (1H, CH_{arom}), 7.31–7.35 m (5H, CH_{arom}), 7.45–7.51 m (4H, CH_{arom}), 7.68 d (2H, CH_{arom}, 3J = 8.1 Hz), 7.75 d (1H, CH_{arom}, 3J = 7.5 Hz), 8.76 s (1H, CH=N), 12.57 s (1H, NH). Anal. calc. for C₂₀H₁₈N₂O₂S, %: C 68.55; H 5.18; N 7.99. Found, %: C 68.51; H 5.09; N 7.91.

3.3. General Procedure for the Synthesis of Complexes **2a–e**

A solution of 0.22 g (1 mmol) of zinc acetate dihydrate in 5 mL of methanol was added to a boiling solution of 2 mmol of azomethine **1a–e** in 20 mL of a mixture of methanol and chloroform (1:1). The reaction was refluxed for 2 h, and then a solution of 0.08 g (2 mmol) of sodium hydroxide in 5 mL of methanol was added dropwise. The precipitate was filtered off, washed with methanol, and dried in a vacuum oven at 100 °C.

Bis [2-[(*E*)-(4-chlorophenyl)iminomethyl]-*N*-(*p*-tolylsulfonyl)anilino]zinc(II) (**2a**) was obtained from 0.77 g of **1a**. Yield 0.58 g (70%), yellow powder, m.p. 317 °C. IR spectrum, ν , cm⁻¹: 1605 (CH=N), 1302 (asSO₂), 1136 (sSO₂). ¹H NMR (DMSO-*d*₆), δ , ppm: 2.30 s (3H, CH₃), 6.92 t (1H, CH_{arom}, 3J = 6.8 Hz), 7.16 d (2H, CH_{arom}, 3J = 8.1 Hz), 7.33 d (4H, CH_{arom}, 3J = 8.7 Hz), 7.42 d (2H, CH_{arom}, 3J = 9.0 Hz), 7.60 d (2H, CH_{arom}, 3J = 8.1 Hz), 7.74 d (1H, CH_{arom}, 3J = 7.2 Hz), 8.76 s (1H, CH=N). Anal. calc. for C₄₀H₃₂Cl₂N₄O₄S₂Zn, %: C 57.67; H 3.87; N 6.72; Zn 7.85. Found, %: C 57.62; H 3.90; N 6.70; Zn 7.81.

Bis[2-[(*E*)-(3,4-dichlorophenyl)iminomethyl]-*N*-(*p*-tolylsulfonyl)anilino]zinc(II) (**2b**) was obtained from 0.84 g of **1b**. Yield 0.69 g (76%), yellow powder, m.p. 304 °C. IR spectrum, ν , cm⁻¹: 1606 (CH=N), 1300 (asSO₂), 1141 (sSO₂). ¹H NMR (DMSO-*d*₆), δ , ppm: 2.30 s (3H,

CH₃), 6.96 t (1H, CH_{arom}, 3J = 7.2 Hz), 7.19 d (2H, CH_{arom}, 3J = 8.1 Hz), 7.25–7.39 m (3H, CH_{arom}), 7.42 d (1H, CH_{arom}, 4J = 1.8 Hz), 7.60 d (1H, CH_{arom}, 3J = 8.4 Hz), 7.67–7.74 m (3H, CH_{arom}), 8.78 s (1H, CH=N). Anal. calc. for C₄₀H₃₀Cl₄N₄O₄S₂Zn, %: C 53.26; H 3.35; N 6.21; Zn 7.25. Found, %: C 53.21; H 3.39; N 6.23; Zn 7.29.

Bis[4-chloro-2-[(E)-(4-chlorophenyl)iminomethyl]-N-(p-tolylsulfonyl)anilino]zinc(II) (**2c**) was obtained from 0.84 g of **1c**. Yield 0.71 g (79%), yellow powder, m.p. 311 °C. IR spectrum, ν , cm⁻¹: 1611 (CH=N), 1301 (asSO₂), 1143 (sSO₂). ¹H NMR (DMSO-*d*₆), δ , ppm: 2.30 s (3H, CH₃), 7.17 d (2H, CH_{arom}, 3J = 8.1 Hz), 7.29–7.33 m (3H, CH_{arom}), 7.39 d (1H, CH_{arom}, 4J = 2.4 Hz), 7.43 d (2H, CH_{arom}, 3J = 8.7 Hz), 7.58 d (2H, CH_{arom}, 3J = 7.8 Hz), 7.87 d (1H, CH_{arom}, 4J = 2.7 Hz), 8.77 s (1H, CH=N). Anal. calc. for C₄₀H₃₀Cl₄N₄O₄S₂Zn, %: C 53.26; H 3.35; N 6.21; Zn 7.25. Found, %: C 53.22; H 3.39; N 6.25; Zn 7.22.

Bis[4-chloro-2-[(E)-(3,4-dichlorophenyl)iminomethyl]-N-(p-tolylsulfonyl)anilino]zinc(II) (**2d**) was obtained from 0.91 g of **1d**. Yield 0.71 g (73%), yellow powder, m.p. 275 °C. IR spectrum, ν , cm⁻¹: 1608 (CH=N), 1295 (asSO₂), 1135 (sSO₂). ¹H NMR (DMSO-*d*₆), δ , ppm: 2.31 s (3H, CH₃), 7.21 d (2H, CH_{arom}, 3J = 8.1 Hz), 7.28 d (2H, CH_{arom}, 3J = 9.3 Hz), 7.41 d (1H, CH_{arom}, 4J = 2.4 Hz), 7.45 s (1H, CH_{arom}), 7.60–7.67 m (3H, CH_{arom}), 7.85 d (1H, CH_{arom}, 4J = 2.4 Hz), 8.77 s (1H, CH=N). Anal. calc. for C₄₀H₂₈Cl₆N₄O₄S₂Zn, %: C 49.48; H 2.91; N 5.77; Zn 6.73. Found, %: C 49.43; H 2.95; N 5.75; Zn 6.78.

Bis[2-[(E)-phenyliminomethyl]-N-(p-tolylsulfonyl)anilino]zinc(II) (**2e**) was obtained from 0.70 g of **1e**. Yield 0.57 g (75%), light yellow powder, m.p. 295–296 °C. IR spectrum, ν , cm⁻¹: 1609 (CH=N), 1285 (asSO₂), 1131 (sSO₂). ¹H NMR (DMSO-*d*₆), δ , ppm: 2.29 s (6H, CH₃), 6.91–6.94 m (2H, CH_{arom}), 7.14 d (4H, CH_{arom}, 3J = 8.1 Hz), 7.31–7.33 m (14H, CH_{arom}), 7.57 d (4H, CH_{arom}, 3J = 7.5 Hz), 7.74 d (2H, CH_{arom}, 3J = 7.8 Hz), 8.74 s (2H, CH=N). Anal. calc. for C₄₀H₃₄N₄O₄S₂Zn, %: C 62.86; H 4.48; N 7.33; Zn 8.56. Found, %: C 62.69; H 4.52; N 7.40; Zn 8.61.

4. Conclusions

A number of azomethine compounds of 2-(*N*-tosylamino)benzaldehyde and 5-chloro-2-(*N*-tosylamino)benzaldehyde with chlorine-substituted anilines and their zinc(II) complexes were synthesized, the structure of which was determined by elemental analysis, IR, ¹H NMR. According to the X-ray absorption spectroscopy data from EXAFS analysis of Zn K-edges, it was found that all complexes have a tetrahedral structure with similar values of Zn ... O/N distances. The PL properties of azomethines and zinc complexes in methylene chloride solution and in solid form have been studied.

It is shown that the introduction of a second chlorine atom into the aniline fragment of the ligand of zinc complexes leads to a slight bathochromic shift of both the UV-Vis absorption maximum and the PL maximum (by 0–3 nm). However, the introduction of a chlorine atom into the aldehyde fragment of the ligand of zinc complexes significantly shifts both the position of the absorption maximum of the UV-Vis spectrum and the maximum of PL by 12–15 nm to the red region. Quantum yields of PL of zinc complexes in the solid-state increase 4–12 times compared to the values in CH₂Cl₂ solutions.

Based on thermogravimetric analysis and differential scanning calorimetry, it was found that all complexes have high thermal stability (290–340 °C). The results of cyclic voltammetry made it possible to determine the energy levels of the complexes. The energy HOMO was –5.21–5.33 eV, with the lower values –5.21–5.33 eV (for **2a** and **2c**) arising from the stronger electron-withdrawing ability of the *meta*-position chlorine atom. TO/PEDOT:PSS/NPD/**2a–d**/TPBI/LiF/AThe LUMO levels are in the range of –2.59 to –2.79 eV. The multilayered devices II were fabricated in which **2a–d** acted as the emitters. The light turn-on voltage for all devices was in the range of 4.5–7 V. All devices emitted a greenish-blue (494 nm for **2a**) or green light (533 nm for **2d**). Complexes **2a** and **2c** with one Cl-atom in the aldehyde fragment of the ligand showed better performance than complexes **2b** and **2d** with two Cl substituents. The devices with **2a** emitter show the highest in this series maximum current and power efficiency of 2.7 cd/A, 1.7 lm/W.

The biological activity of azomethines and zinc complexes has been studied. Azomethins **1a**, **1b**, and **1d** had the highest antibacterial activity, but their activity was 2 times weaker than that of the reference drug furazolidone. In the case of complexes, the protistocidal activity of the complex of zinc with azomethine of 5-chloro-2-(*N*-tosylamino)benzaldehyde with 4-chloroaniline **2c** was two times higher than the activity of toltrazuril. The obtained results of the study of biological activity allow us to conclude that the search for antiprotozoal drugs among azomethines of halogen-substituted 2-(*N*-tosylamino)benzaldehyde with halogen-containing anilines and metal complexes based on them is promising.

Supplementary Materials: The following supporting information can be downloaded at: <https://www.mdpi.com/article/10.3390/ijms232315259/s1>.

Author Contributions: Conceptualization, A.S.B. and Y.V.K.; investigation, V.G.V., M.S.M., N.I.M., A.A.Z., D.A.G. and A.N.G.; data curation, V.A.L. and A.L.T.; writing—original draft preparation, A.S.B. and V.G.V.; writing—review and editing, A.A.K. and W.L.; visualization, V.G.V.; project administration, A.V.M. All authors have read and agreed to the published version of the manuscript.

Funding: This research was funded by the Ministry of Science and Higher Education of the Russian Federation (State assignment in the field of scientific activity, Southern Federal University, 0852-2020-0031) and federal program Prioritet-2030 (Crimean Federal University V.I. Vernadsky).

Institutional Review Board Statement: Not applicable.

Informed Consent Statement: Not applicable.

Data Availability Statement: The data presented in this article are openly available.

Acknowledgments: IR and ¹H NMR spectra were obtained using facilities of the “Molecular Spectroscopy” Multi-user Center of Southern Federal University.

Conflicts of Interest: The authors declare no conflict of interest.

References

1. Vigato, P.A.; Tamburini, S. The challenge of cyclic and acyclic Schiff bases and related derivatives. *Coord. Chem. Rev.* **2004**, *248*, 1717–2128. [[CrossRef](#)]
2. Vigato, P.A.; Tamburini, S.; Bertolo, L. The development of compartmental macrocyclic Schiff bases and related polyamine derivatives. *Coord. Chem. Rev.* **2007**, *251*, 1311–1492. [[CrossRef](#)]
3. Vigato, P.A.; Tamburini, S. Advances in acyclic compartmental ligands and related complexes. *Coord. Chem. Rev.* **2008**, *252*, 1871–1995. [[CrossRef](#)]
4. Arunadevi, A.; Raman, N. Biological response of Schiff base metal complexes incorporating amino acids—A short review. *J. Coord. Chem.* **2020**, *73*, 2095–2116. [[CrossRef](#)]
5. Loginova, N.V.; Harbatsevich, H.I.; Osipovich, N.P.; Ksendzova, G.A.; Koval’chuk, T.V.; Polozov, G.I. Metal Complexes as Promising Agents for Biomedical Applications. *Curr. Med. Chem.* **2020**, *27*, 5213–5249. [[CrossRef](#)]
6. Vlasenko, V.G.; Burlov, A.S.; Koshchienko, Y.V.; Kiskin, M.A.; Garnovskii, D.A.; Zubavichus, Y.V.; Kolodina, A.A.; Trigub, A.L.; Zubenko, A.A.; Drobin, Y.D. Synthesis, characterization, and biological activity of Co(II), Ni(II), and Cu(II) complexes derived from *N,N'*-bis(2-*N*-tosylaminobenzylidene)diaminodipropyliminatate ligand. *Inorg. Chim. Acta* **2020**, *510*, 119776. [[CrossRef](#)]
7. Burlov, A.S.; Vlasenko, V.G.; Koshchienko, Y.V.; Makarova, N.I.; Zubenko, A.A.; Drobin, Y.D.; Fetisov, L.N.; Kolodina, A.A.; Zubavichus, Y.V.; Trigub, A.L.; et al. Synthesis, characterization, luminescent properties and biological activities of zinc complexes with bidentate azomethine Schiff-base ligands. *Polyhedron* **2018**, *154*, 65–76. [[CrossRef](#)]
8. Adhikary, C.; Banerjee, S.; Chakraborty, J.; Ianelli, S. Copper(II) azide complexes with NNO donor ligands: Syntheses, structure, catalysis and biological studies. *Polyhedron* **2013**, *65*, 48–53. [[CrossRef](#)]
9. Garoufis, A.; Hadjikakou, S.K.; Hadjiliadis, N. Palladium coordination compounds as anti-viral, anti-fungal, anti-microbial and anti-tumor agents. *Coord. Chem. Rev.* **2009**, *253*, 1384–1397. [[CrossRef](#)]
10. Chen, H.Q.; Hall, S.; Zheng, B.; Rhodes, J. Potentiation of the immune system by Schiff-base forming drugs: Mechanism of action and therapeutic potential. *Biodrugs* **1997**, *7*, 217–231. [[CrossRef](#)]
11. Parsekar, S.U.; Haldar, P.; Antharjanam, P.K.S.; Kumar, M.; Koley, A.P. Synthesis, characterization, crystal structure, DNA and human serum albumin interactions, as well as antiproliferative activity of a Cu(II) complex containing a Schiff base ligand formed in situ from the Cu(II)-induced cyclization of 1,5-bis(salicylidene)thiocarbohydrazide. *Appl. Organomet. Chem.* **2021**, *35*, e6152. [[CrossRef](#)]

12. Kargar, H.; Behjatmanesh-Ardakani, R.; Torabi, V.; Sarvian, A.; Kazemi, Z.; Chavoshpour-Natanzi, Z.; Mirkhani, V.; Sahraei, A.; Tahir, M.N.; Ashfaq, M. Novel copper(II) and zinc(II) complexes of halogenated bidentate N,O-donor Schiff base ligands: Synthesis, characterization, crystal structures, DNA binding, molecular docking, DFT and TD-DFT computational studies. *Inorg. Chim. Acta* **2021**, *514*, 120004. [[CrossRef](#)]
13. Ribeiro, N.; Bulut, I.; Cevatemre, B.; Teixeira, C.; Yildizhan, Y.; Andre, V.; Adao, P.; Pessoa, J.C.; Acilan, C.; Correia, I. Cu(II) and V(IV)O complexes with tri- or tetradentate ligands based on (2-hydroxybenzyl)-l-alanines reveal promising anticancer therapeutic potential. *Dalton Trans.* **2021**, *50*, 157–169. [[CrossRef](#)] [[PubMed](#)]
14. Shah, S.S.; Shah, D.; Khan, I.; Ahmad, S.; Ali, U.; Rahman, A.U. Synthesis and Antioxidant Activities of Schiff Bases and Their Complexes: An Updated Review. *Res. Appl. Chem.* **2020**, *10*, 6936–6963. [[CrossRef](#)]
15. Deda, M.D.; Ghedini, M.; Aiello, I.; Grisolia, A. A new blue photoluminescent Salen-like zinc complex with excellent emission quantum yield. *Chem. Lett.* **2004**, *33*, 1060–1061. [[CrossRef](#)]
16. Kaplunov, M.G.; Krasnikova, S.S.; Yakushchenko, I.K.; Shamaev, S.N.; Pivovarov, A.P.; Efimov, O.N. New organic electroluminescent materials. *Mol. Cryst. Liq. Cryst.* **2005**, *426*, 287–293. [[CrossRef](#)]
17. Yu, T.; Su, W.; Li, W.; Hong, Z.; Hua, R.; Li, M.; Chu, B.; Li, B.; Zhang, Z.; Hu, Z.Z. Synthesis, crystal structure and electroluminescent properties of a Schiff base zinc complex. *Inorg. Chim. Acta* **2006**, *359*, 2246–2251. [[CrossRef](#)]
18. Xie, J.; Qiao, J.; Wang, L.; Xie, J.; Qiu, Y. An azomethine-zinc complex for organic electroluminescence: Crystal structure, thermal stability and optoelectronic properties. *Inorg. Chim. Acta* **2005**, *358*, 4451–4458. [[CrossRef](#)]
19. Chen, L.; Qiao, J.; Xie, J.; Duan, L.; Zhang, D. Substituted azomethine-zinc complexes: Thermal stability, electrochemical and electron transport properties. *Inorg. Chim. Acta* **2009**, *362*, 2327–2333. [[CrossRef](#)]
20. Kotova, O.V.; Eliseeva, S.V.; Averjushkin, A.S.; Lepnev, L.S.; Vaschenko, A.A.; Rogachev, A.Y.; Vitukhnovsky, A.G.; Kuzmina, N.P. Zinc(II) complexes with Schiff bases derived from ethylenediamine and salicylaldehyde: The synthesis and photoluminescent properties. *Russ. Chem. Bull. Intern. Ed.* **2008**, *57*, 1880–1889. [[CrossRef](#)]
21. Chen, C.H.; Shi, J. Metal chelates as emitting materials for organic electroluminescence. *Coord. Chem. Rev.* **1998**, *171*, 161–174. [[CrossRef](#)]
22. Gusev, A.N.; Braga, E.; Shul'gin, V.; Lyssenko, K.; Eremenko, I.; Samsonova, L.; Degtyarenko, K.; Kopylova, T.; Linert, W. Luminescent Properties of Zn and Mg Complexes on N-(2-Carboxyphenyl)salicylideneimine Basis. *Materials* **2017**, *10*, 897. [[CrossRef](#)]
23. Kotova, O.; Lyssenko, K.; Rogachev, A.; Eliseeva, S.; Fedyanin, I.; Lepnev, L.; Pandey, L.; Burlov, A.; Garnovskii, A.; Vitukhnovsky, A.; et al. Low temperature X-ray diffraction analysis, electronic density distribution and photophysical properties of bidentate N,O-donor salicylaldehyde Schiff bases and zinc complexes in solid state. *J. Photochem. Photobiol. A Chem.* **2011**, *218*, 117–129. [[CrossRef](#)]
24. Burlov, A.S.; Vlasenko, V.G.; Koshchienko, Y.V.; Makarova, N.I.; Zubenko, A.A.; Drobin, Y.D.; Borodkin, G.S.; Metelitsa, A.V.; Zubavichus, Y.V.; Garnovskii, D.A. Complexes of zinc(II) with N-2-(hydroxyalkyliminomethyl)phenyl-4-methylbenzenesulfonamides: Synthesis, structure, photoluminescence properties and biological activity. *Polyhedron* **2018**, *144*, 249–258. [[CrossRef](#)]
25. Burlov, A.S.; Mal'tsev, E.I.; Vlasenko, V.G.; Garnovskii, D.A.; Dmitriev, A.V.; Lypenko, D.A.; Vannikov, A.V.; Dorovatovskii, P.V.; Lazarenko, V.A.; Zubavichus, Y.V.; et al. Synthesis, structure, photo- and electroluminescent properties of bis{(4-methyl-N-2-(E)-2-pyridyliminomethylphenyl)benzenesulfonamide}zinc(II). *Polyhedron* **2017**, *133*, 231–237. [[CrossRef](#)]
26. Burlov, A.S.; Vlasenko, V.G.; Dmitriev, A.V.; Chesnokov, V.V.; Uraev, A.I.; Garnovskii, D.A.; Zubavichus, Y.V.; Trigub, A.L.; Vasilchenko, I.S.; Lypenko, D.A.; et al. Synthesis, structure, photo- and electroluminescent properties of zinc(II) complexes with aminomethylene derivatives of 1-phenyl-3-methyl-4-formylpyrazol-5-one and 3- and 6-aminoquinolines. *Synth. Metals* **2015**, *203*, 156–163. [[CrossRef](#)]
27. Burlov, A.S.; Koshchienko, Y.V.; Makarova, N.I.; Kuz'menko, T.A.; Chesnokov, V.V.; Kiskin, M.A.; Nikolaevskii, S.A.; Garnovskii, D.A.; Uraev, A.I.; Vlasenko, V.G.; et al. Mixed-ligand Zn(II) complexes of 1-phenyl-3-methyl-4-formylpyrazole-5-one and various aminoheterocycles: Synthesis, structure and photoluminescence properties. *Synth. Metals* **2016**, *220*, 543–550. [[CrossRef](#)]
28. Gusev, A.N.; Braga, E.V.; Kryukova, M.A.; Lyubomirskii, N.V.; Zamnius, E.A.; Shul'gin, V.F. Photoluminescence of the Coordination Zinc Compounds with 3-Methyl-4-Formyl-1-Phenylpyrazol-5-one Acylhydrazones. *Russ. J. Coord. Chem.* **2020**, *46*, 251–259. [[CrossRef](#)]
29. Gusev, A.N.; Kiskin, M.A.; Braga, E.V.; Kryukova, M.A.; Baryshnikov, G.V.; Karaush-Karmazin, N.N.; Minaeva, V.A.; Minaev, B.F.; Ivaniuk, K.; Stakhira, P.; et al. Schiff Base Zinc(II) Complexes as Promising Emitters for Blue Organic Light-Emitting Diodes. *ACS Appl. Electron. Mater.* **2021**, *3*, 3436–3444. [[CrossRef](#)]
30. Gusev, A.N.; Kiskin, M.A.; Braga, E.V.; Chapran, M.; Wiosna-Salyga, G.; Baryshnikov, G.V.; Minaeva, V.A.; Minaev, B.F.; Ivaniuk, K.; Stakhira, P.; et al. Novel Zinc Complex with an Ethylenediamine Schiff Base for High-Luminance Blue Fluorescent OLED Applications. *J. Phys. Chem. C* **2019**, *123*, 11850–11859. [[CrossRef](#)]
31. Burlov, A.S.; Vlasenko, V.G.; Koshchienko, Y.V.; Makarova, N.I.; Kiskin, M.A.; Kolodina, A.A.; Garnovskii, D.A.; Trigub, A.L.; Metelitsa, A.V. Chemical and electrochemical synthesis, structure, photoluminescent properties, and biological activity of 4-methyl-N-2-(Z)-2-(2-pyridyl)alkyliminomethylphenylbenzenesulfamide zinc(II) complexes. *Appl. Organometal. Chem.* **2020**, *34*, e5302. [[CrossRef](#)]

32. Burlov, A.S.; Vlasenko, V.G.; Makarova, N.I.; Lyssenko, K.A.; Chesnokov, V.V.; Borodkin, G.S.; Vasilchenko, I.S.; Uraev, A.I.; Garnovskii, D.A.; Metelitsa, A.V. Chemical and electrochemical synthesis, molecular structures, DFT calculations and optical properties of metal-chelates of 8-(2-tosylaminobenzilideneimino)quinolone. *Polyhedron* **2016**, *107*, 153–162. [[CrossRef](#)]
33. Burlov, A.S.; Vlasenko, V.G.; Koshchienko, Y.V.; Milutka, M.S.; Garnovskii, D.A.; Kolodina, A.A.; Zubavichus, Y.V.; Kiskin, M.A. Synthesis, structure, and photoluminescence of Zn(II) and Cd(II) complexes with N-2-(diethylaminoalkyliminomethyl)-phenyl-4-methylbenzenesulfonamides. *Polyhedron* **2021**, *208*, 115400. [[CrossRef](#)]
34. Burlov, A.S.; Vlasenko, V.G.; Koshchienko, Y.V.; Milutka, M.S.; Mal'tsev, E.I.; Dmitriev, A.V.; Lypenko, D.A.; Nekrasova, N.V.; Kolodina, A.A.; Makarova, N.I.; et al. Synthesis, structure, and photoluminescent and electroluminescent properties of zinc(II) complexes with bidentate azomethine ligands. *Appl. Organomet. Chem.* **2021**, *35*, e6107. [[CrossRef](#)]
35. Milutka, M.S.; Burlov, A.S.; Vlasenko, V.G.; Koshchienko, Y.V.; Makarova, N.I.; Metelitsa, A.V.; Korshunova, E.V.; Trigub, A.L.; Zubenko, A.A.; Klimenko, A.I. Synthesis, Structure, Spectral-Luminescent Properties, and Biological Activity of Chlorine-Substituted Azomethines and Their Zinc(II) Complexes. *Russ. J. Gen. Chem.* **2021**, *91*, 1706–1716. [[CrossRef](#)]
36. Milutka, M.S.; Burlov, A.S.; Vlasenko, V.G.; Koshchienko, Y.V.; Korshunova, E.V.; Uraev, A.I.; Trigub, A.L.; Zubenko, A.A.; Klimenko, A.I.; Gusev, A.N. Zinc(II) Complexes with Azomethines of 2,4,6-Trimethylaniline and Halogen-Substituted Salicylaldehyde. *Russ. J. Gen. Chem.* **2022**, *92*, 1297–1308. [[CrossRef](#)]
37. Groom, C.R.; Bruno, I.J.; Lightfoot, M.P.; Ward, S.C. The Cambridge Structural Database. *Acta Cryst. B* **2016**, *72*, 171–179. [[CrossRef](#)]
38. Oloyede-Akinsulere, A.I.; Babajide, J.O.; Salihu, S.O. Synthesis, Antibacterial and Antioxidant Activities of Some Tridentate Substituted Salicylaldimines. *Asian J. Appl. Chem. Res.* **2018**, *1*, 43067. [[CrossRef](#)]
39. Al-Shboul, T.M.A.; El-khateeb, M.; Obeidat, Z.H.; Ababneh, T.S.; Al-Tarawneh, S.S.; Al Zoubi, M.S.; Alshaer, W.; Abu Seni, A.; Qasem, T.; Moriyama, H.; et al. Synthesis, Characterization, Computational and Biological Activity of Some Schiff Bases and Their Fe, Cu and Zn Complexes. *Inorganics* **2022**, *10*, 112. [[CrossRef](#)]
40. Krasovitskii, B.M.; Bolotin, B.M. *Organicheskie lyuminofory Organic Luminophores*; Khimiya: Moscow, Russia, 1984; p. 292. (In Russian)
41. Gusev, A.; Shul'gin, V.; Braga, E.; Zamnius, E.; Kryukova, M.; Linert, W. Luminescent properties of Zn complexes based on tetradentate N2O2 -donor pyrazolone schiff bases. *Dyes Pigm.* **2020**, *183*, 108626–108632. [[CrossRef](#)]
42. Chernyshov, A.A.; Veligzhanin, A.A.; Zubavichus, Y.V. Structural Materials Science End-Station at the Kurchatov Synchrotron Radiation Source: Recent Instrumentation Upgrades and Experimental Results. *Nucl. Instr. Meth. Phys. Res. A* **2009**, *603*, 95–98. [[CrossRef](#)]
43. Newville, M. EXAFS analysis using FEFF and FEFFIT. *J. Synchrotron Rad.* **2001**, *8*, 96–100. [[CrossRef](#)] [[PubMed](#)]
44. Zabinski, S.I.; Rehr, J.J.; Ankudinov, A.; Alber, R.C. Multiple-scattering calculations of x-ray-absorption spectra. *Phys. Rev.* **1995**, *52*, 2995–3011. [[CrossRef](#)] [[PubMed](#)]
45. Lazarenko, V.A.; Dorovatovskii, P.V.; Zubavichus, Y.V.; Burlov, A.S.; Koshchienko, Y.V.; Vlasenko, V.G.; Khrustalev, V.N. High-throughput small-molecule crystallography at the 'Belok' beamline of the Kurchatov synchrotron radiation source: Transition metal complexes with azomethine ligands as a case study. *Crystals* **2017**, *7*, 325. [[CrossRef](#)]
46. Svetogorov, R.D.; Dorovatovskii, P.V.; Lazarenko, V.A. Belok/XSA diffraction beamline for studying crystalline samples at Kurchatov Synchrotron Radiation Source. *Cryst. Res. Technol.* **2020**, *55*, 1900184. [[CrossRef](#)]
47. Kabsch, W. XDS. *Acta Crystallogr. Sect. D Bio. Crystallogr.* **2010**, *66*, 125–132. [[CrossRef](#)]
48. Sheldrick, G.M. SHELXT—Integrated space-group and crystal-structure determination. *Acta Crystallogr. Sect. A Found Adv.* **2015**, *71*, 3–8. [[CrossRef](#)]
49. Dolomanov, O.V.; Bourhis, L.J.; Gildea, R.J.; Howard, J.A.; Puschmann, H. OLEX2: A complete structure solution, refinement and analysis program. *J. Appl. Crystallogr.* **2009**, *42*, 339–341. [[CrossRef](#)]
50. Sheldrick, G.M. Crystal structure refinement with SHELXL. *Acta Crystallogr. Sect. C Struct. Chem.* **2015**, *71*, 3–8. [[CrossRef](#)]